

Electronic and optical properties of spinel zinc ferrite: *Ab initio* hybrid functional calculations

Daniel Fritsch

Department of Chemistry, University of Bath, Claverton Down, Bath BA2 7AY, United Kingdom

(Dated: July 3, 2021)

Spinel ferrites in general show a rich interplay of structural, electronic, and magnetic properties. Here, we particularly focus on zinc ferrite (ZFO), which has been observed experimentally to crystallise in the cubic *normal* spinel structure. However, its magnetic ground state is still under dispute. In addition, some unusual magnetic properties in ZFO thin films or nanostructures have been explained by a possible partial cation inversion and a different magnetic interaction between the two cation sublattices of the spinel structure compared to the crystalline bulk material. Here, density functional theory has been applied to investigate the influence of different inversion degrees and magnetic couplings among the cation sublattices on the structural, electronic, magnetic, and optical properties. Effects of exchange and correlation have been modelled using the generalised gradient approximation (GGA) together with the Hubbard “+ U ” parameter, and the more elaborate hybrid functional PBE0. While the GGA+ U calculations yield an antiferromagnetically coupled *normal* spinel structure as the ground state, in the PBE0 calculations the ferromagnetically coupled *normal* spinel is energetically slightly favoured, and the hybrid functional calculations perform much better with respect to structural, electronic and optical properties.

PACS numbers: 71.15.Mb, 71.20.Nr, 78.20.Bh

Zinc ferrite or ZnFe_2O_4 (ZFO) belongs to the mineral class of spinel ferrites crystallising in a cubic crystal structure with the general formula $M\text{Fe}_2\text{O}_4$. Common to all spinel ferrites is the face-centred cubic (fcc) arrangement of the oxygen anions. In the so-called *normal* spinel structure the octahedrally coordinated B-sites (O_h) are solely populated with Fe^{3+} cations whereas the tetrahedrally coordinated A-sites (T_d) accommodate a divalent d -metal cation, e.g., $M \in \text{Mn, Fe, Co, Ni, Cu, Zn, Mg, Cd}$.¹ One also finds mixed-valence occupancies, $(M_{1-\lambda}\text{Fe}_\lambda)[M_\lambda\text{Fe}_{2-\lambda}]\text{O}_4$, with the inversion parameter λ ranging from $\lambda = 0$ for the *normal* to $\lambda = 1$ for the so-called *inverse* spinel. Combining a divalent cation with a non-integer inversion degree, which can partly be tailored by experimental growth conditions,² offers a huge variety of structural, electronic, and magnetic properties within the mineral class of spinel ferrites.

An example for a fully *inverse* spinel ferrite is NiFe_2O_4 (NFO), whereas CoFe_2O_4 (CFO) has a partially inverse structure with $\lambda \approx 0.8$.³ Both, NFO and CFO, are ferro(i)magnetic (FM) insulators with high Curie temperatures and large saturation magnetisations,⁴ with possible applications in artificial multiferroic heterostructures or spintronics devices.⁵ An example for a *normal* spinel is ZFO. Although experimentally mostly reported to be an antiferromagnetic (AFM) insulator, with a comparatively low Néel temperature of $T_N \approx 10$ K,^{3,6,7} there is still an ongoing discussion about its magnetic ground state. While very early models suggested various AFM arrangements of the magnetic moments among the A- and B-site sublattices,^{8–11} in recent experiments on high-quality single crystals, no AFM order has been observed for temperatures down to 1.5 K, and the AFM order is actually thought to originate from defects or inhomogeneities.¹²

This makes the magnetic structure of spinel ferrites particularly interesting, e.g. the interactions among the magnetic cations distributed over the A- and B-sites, and possible phase transitions. A first understanding of the magnetic interactions in spinels was provided by the Néel model¹³ which described a collinear arrangement of magnetic moments among the A- and B-site sublattices. This is realised, e.g., in NFO and CFO, where the A- and B-site cations order ferromagnetically among themselves, and antiferromagnetically with respect to the other sublattice. With the d^5 (Fe^{3+}) and d^7 (Co^{2+}) “levels” of d -orbital population the additional choice of high-spin vs low-spin complexes arises. However, for the tetrahedrally coordinated A-sites only high-spin complexes are observed, and within the mentioned materials the B-sites have high-spin complexes as well. Different inversion degrees combined with possible high-spin vs low-spin complexes add another complication to properly describe the correct magnetic ground state of spinel ferrites. With a non-magnetic cation (such as Zn^{2+} in ZFO) populating the A-sites it becomes more favourable for the Fe^{3+} cations to order antiferromagnetically on the B-sites below 10 K; contrary to the ferromagnetic coupling in NFO, CFO, and ZFO at higher temperatures.^{3,7}

In addition, contrary to the *normal* spinel ground state of bulk ZFO, several properties in strained thin films and nanoparticles, like increased magnetisation, have been explained based on a partial inversion and/or a AFM to FM change in the B-site magnetisation. Experimental works so far dealt with single crystals,¹² epitaxial thin films,^{2,14–17} and nanocrystalline samples,^{18,19} respectively. The optical properties of ZFO have only been rarely investigated.^{15,17,20,21} Available theoretical works focused on the ground state properties of ZFO using various exchange-correlation functionals, includ-

ing variants of the generalised gradient approximation (GGA),^{22–24} different parametrisations of the GGA+ U functional,^{16,22,25} and a recent GGA plus many-body correction investigation,²¹ respectively. Although more elaborate hybrid functionals have proven to give improved results for other spinel ferrites,²⁶ systematic studies for ZFO are missing to date.

Here, we focus on differences between the *collinear* AFM and FM *normal* spinel structure, as well as inverse structures with $\lambda = 0.5$ and $\lambda = 1.0$. Presented results include structural (lattice constant a , oxygen parameter u , bulk modulus B), electronic (density of states (DOS), band structure), magnetic, and optical (dielectric functions) properties.

I. COMPUTATIONAL DETAILS

The results of the present work have been obtained by density functional theory (DFT) calculations employing the Vienna *ab initio* Simulation package (VASP)^{27–29} together with the projector-augmented wave (PAW) formalism.³⁰ Spin-polarisation has been taken into account. Standard VASP PAW potentials were used with 14, 12, and 6 valence electrons for iron, zinc, and oxygen, respectively. Approximations to the exchange-correlation potential used in the present work are the GGA together with Hubbard “+ U ” method³¹ based on the Perdew-Burke-Ernzerhof (PBE) parametrisation,³² and the more elaborate hybrid functional PBE0,³³ where a quarter of the exchange potential is replaced by Hartree-Fock exact-exchange. The Hubbard “+ U ” method has been applied in the simplified, rotationally invariant version of Dudarev *et al.*,³⁴ with a value of $U_{\text{eff}} = U - J = 5.25$ eV applied to the Fe cations. This value of U_{eff} has been chosen to reproduce the experimental band gap of ZFO of around 2.2 eV,^{35,36} is similar to the $U_{\text{eff}} = 5.9$ eV applied to FeO³¹ and is slightly larger than $U_{\text{eff}} = 3$ eV applied to NFO and CFO.^{4,37} Both functionals, the GGA+ U and the hybrid PBE0, are employed to overcome the insufficient description of electronic exchange effects in standard DFT calculations.^{31,33}

The spinel structure crystallises in the cubic space group $Fd\bar{3}m$ (No. 227) with the smallest possible unit cell accomodating two functional units (f.u.) of ZFO and 14 atoms. Due to the necessary application of periodic boundary conditions, the calculations face an artificial symmetry reduction depending on the chosen inversion degree and magnetic order.^{4,38,39} Similar to our earlier works on spinel ferrites, structural relaxations were performed for several volumes of the smallest possible unit cell within a scalar-relativistic approximation and allowing the internal structure parameter to relax until all forces on the atoms were smaller than $0.001 \text{ eV}\text{\AA}^{-1}$. Dense Γ -centred k point meshes of $8 \times 8 \times 8$ for the Brillouin zone integration and a cutoff energy of 800 eV ensured converged structural parameters and total energies within meV accuracy for the GGA+ U calculations.

For the more demanding PBE0 calculations, Γ -centred k point meshes of $6 \times 6 \times 6$ and a cutoff energy of 500 eV have been used. Ground-state geometries were determined by a cubic spline fit to the total energies with respect to the unit cell volumes.

II. RESULTS AND DISCUSSION

The obtained structural properties of ZFO are given in table I in comparison to available experimental results. The GGA+ U calculated lattice constants, oxygen parameters u , and bulk moduli for the *normal* spinel are 8.541 \AA , 0.261, and 161.1 GPa, and 8.545 \AA , 0.260, and 162.0 GPa for the AFM and FM arrangement of magnetic moments among the B-site sublattice, respectively. The respective PBE0 calculated lattice constants, oxygen parameters u , and bulk moduli are 8.446 \AA , 0.261, and 173.8 GPa, and 8.452 \AA , 0.260, 174.1 GPa, and are in much better agreement to the experimental results of 8.441 \AA [40] (8.4599 \AA [6]), 0.260 [41], and 175.0 GPa [42], respectively. This is in line with the general trend that hybrid functional calculations for oxide semiconductors yield better agreement of lattice parameters and bulk moduli with respect to experimental results.⁴³

The AFM arrangement of magnetic moments among the B-site sublattice is the ground state for the GGA+ U calculations, in agreement with experiment and other theoretical investigations, whereas the FM arrangement is slightly favoured for the hybrid functional PBE0 calculations.

As can be seen from the data in table I, with increasing inversion degree λ the lattice constants decrease from the *normal* spinel AFM values for both, GGA+ U and PBE0 functional calculations, in agreement with experimental results of Wu *et al.*,¹⁹ who report a lattice constant of 8.377 \AA for a partially inverse ZFO sample with $\lambda = 0.5$. Both, the GGA+ U and PBE0 calculated bulk moduli increase with increasing inversion degree λ .

The DOS of *normal* ZFO with a AFM and FM arrangement of magnetic moments among the B-site sublattices, partially inverse ZFO ($\lambda = 0.5$) and fully inverse ZFO ($\lambda = 1.0$) are shown in figure 1. The left and right panels depict the results of GGA+ U and PBE0 calculations, and the zero energy is set to the valence band maximum, respectively. In each of the panels the total DOS is shown as shaded grey area, and the spin-up (spin-down) contributions are given along the positive (negative) y -axis. Generally, apart from the larger band gap for the PBE0 calculations, the overall shape of the DOS looks quite similar for the GGA+ U and the PBE0 calculations.

From the DOS with respect to the inversion degree λ it can be seen that an increasing inversion degree shifts the valence band DOS towards higher energies, and exhibits a growing contribution to the tetrahedral Fe and octahedral Zn DOS, respectively. From figure 1 it can also be seen that both, GGA+ U and PBE0 calculations, yield

TABLE I. Ground state structural properties (lattice constant a , oxygen parameter u , and bulk modulus B) of ZFO calculated with the GGA+ U and PBE0 exchange-correlation functionals and different inversion degrees λ in comparison to available experimental results. The theoretical data also includes the energy difference ΔE with respect to the most stable configuration. For the *normal* spinel ($\lambda = 0.0$) the first (second) data set reports structural properties for the AFM (FM) arrangement of magnetic moments among the B-site sublattice, respectively.

λ	GGA+ U				PBE0				Expt.		
	a [Å]	u	B [GPa]	ΔE [eV]	a [Å]	u	B [GPa]	ΔE [eV]	a [Å]	u	B [GPa]
0.0	8.541	0.261	161.1	0.0	8.446	0.261	173.8	0.030	8.441 [40]	0.260 [41]	175.0 [42]
	8.52 [22]			0.0 [22]					8.4599 [6]		
0.0	8.545	0.260	162.0	0.051	8.452	0.260	174.1	0.0			
	8.53 [22]			0.068 [22]							
0.5	8.526	0.259	166.3	0.519	8.424	0.259	192.6	0.175	8.377 [19]		
1.0	8.515	0.250	169.8	0.761	8.407	0.250	203.7	0.213			
	8.49 [22]			0.210 [22]							

an insulating behaviour, underlying the important effect of electronic exchange effects on the electronic properties compared to plain GGA approaches.⁴⁴

The local magnetic moments for Fe cations are found to be in the range of 4.1 to 4.3 μ_B , with the GGA+ U values being slightly larger than the PBE0 ones, for all inversion degrees and arrangements of magnetic moments among the B-site sublattices. This is in favourable agreement with the experimental value of 4.22 μ_B [6] and the range of 4.1 to 4.2 μ_B reported from other GGA+ U calculations,²² respectively.

For the *normal* spinel and AFM arrangement of magnetic moments among the B-site sublattice it is no surprise that the spin resolved band structure depicted in the upper panels of figure 2 shows the same behaviour for the spin-up and spin-down channels, with a band gap of 2.21 eV (3.68 eV) for the GGA+ U (PBE0) calculations. While the GGA+ U band gap is close to the experimental band gap of around 2.2 eV,^{35,36} the PBE0 band gap is close to the experimental band gap of 3.31 eV, obtained from spectroscopic ellipsometry measurements.¹⁵ This changes drastically for the FM arrangement, where the band gap is now between the spin-up valence band and the spin-down conduction band for both, and amounts to 1.68 eV (3.13 eV) for the GGA+ U (PBE0) calculations, respectively. Changing the inversion degree λ from 0.5 to 1.0 only has a small influence on the band gap, which is now around 1.91 eV (3.37 eV) for the GGA+ U (PBE0) calculations.

Based on the obtained relaxed structural ground states for different inversion degrees λ and magnetic arrangements on the B-site sublattices the optical properties have been calculated and are depicted in figure 3. Generally, the onsets of the imaginary parts of the PBE0 dielectric functions (ε_2) are shifted towards higher energies, as to be expected from the larger band gaps already seen in the DOS (figure 1) and the band structures (fig-

ure 2). Moreover, all the PBE0 dielectric functions are flatter compared to the GGA+ U ones. If one accounts for the slight changes in the observed band gaps, the overall features of the imaginary part of the PBE0 dielectric function for *normal* ZFO and a AFM arrangement of the magnetic moment among the B-site cations (upper right panel of figure 3), is in good agreement with the optical data reported in.¹⁵

III. SUMMARY AND OUTLOOK

In summary, a detailed investigation on the influence of the inversion degree λ and different arrangements of the magnetic moments among the B-site cations on the structural, electronic, magnetic, and optical properties of the spinel ferrite ZFO has been presented. It has been shown that the hybrid functional PBE0 performs better than GGA+ U , and yields an overall better agreement with respect to experimental results on structural, electronic and optical properties. These hybrid functional calculations provide the basis for future in-depth analyses of the optical properties in relation to the band structure and DOS, as well as taking into account strain effects from underlying substrates.^{4,39}

ACKNOWLEDGMENTS

This research has received funding from the European Unions Horizon 2020 research and innovation programme under grant agreement No 641864 (INREP). This work made use of the ARCHER UK National Supercomputing Service (<http://www.archer.ac.uk>) via the membership of the UKs HPC Materials Chemistry Consortium, funded by EPSRC (EP/L000202) and the Balena HPC facility of the University of Bath.

¹ J. Smit and H. P. J. Wijn, *Ferrites* (Cleaver-Hume Press, London, 1959).

² Y. F. Chen, D. Spoddig, and M. Ziese, *J. Phys. D: Appl. Phys.* **41**, 205004 (2008).

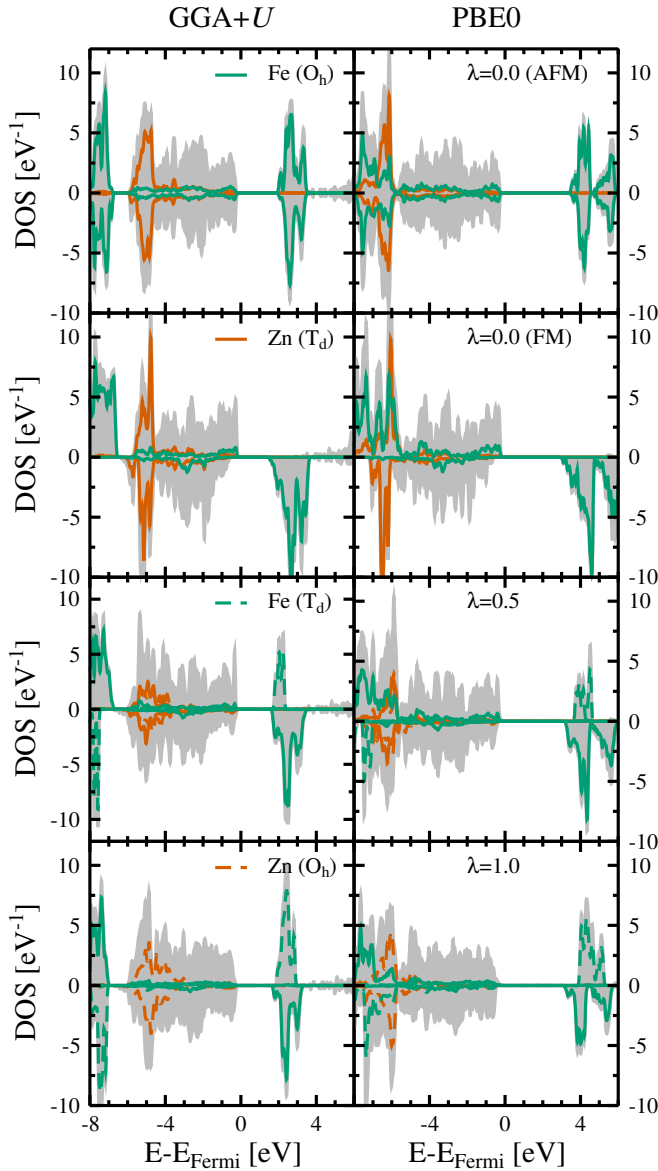


FIG. 1. (Color online) Total and projected DOS per formula unit for ZFO calculated with the GGA+ U (left panels) and PBE0 (right panels) exchange-correlation functionals for different inversion degrees λ and arrangements of the magnetic moments among the B-site sublattice, respectively. The octahedral O_h (tetrahedral T_d) states of Fe are shown as straight (dashed) green lines, and the tetrahedral T_d (octahedral O_h) states of Zn are shown as straight (dashed) red lines, respectively. The shaded grey area in all panels depicts the total DOS. Minority spin projections are shown using negative values. The zero energy is set to the valence band maximum.

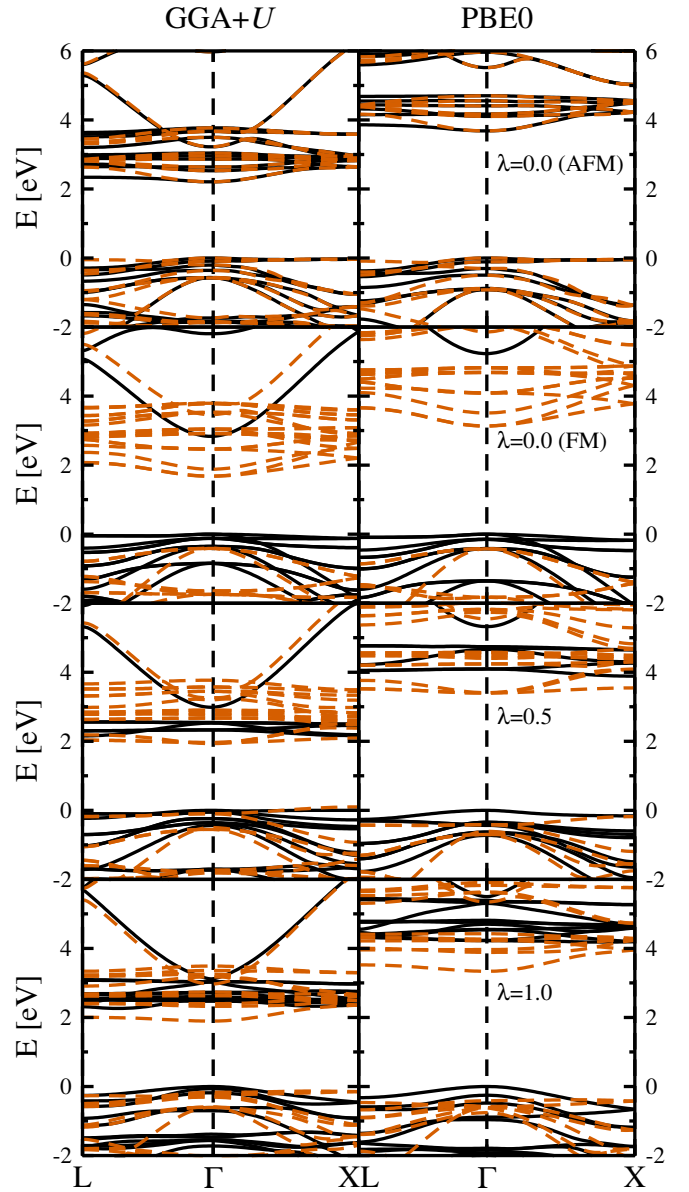


FIG. 2. (Color online) Electronic band structures for ZFO calculated with the GGA+ U (left panels) and PBE0 (right panels) exchange-correlation functionals for different inversion degrees λ and arrangements of the magnetic moments among the B-site sublattice, respectively. Majority- and minority-spin bands are shown as full (black) and dashed (red) lines. The zero energy is set to the valence band maximum.

³ V. A. M. Brabers, in *Handbook of Magnetic Materials*, Vol. 8, edited by K. H. J. Buschow (Elsevier, 1995) pp. 189 – 324.

⁴ D. Fritsch and C. Ederer, *Phys. Rev. B* **82**, 104117 (2010).

⁵ N. Caffrey, D. Fritsch, T. Archer, S. Sanvito, and C. Ederer, *Phys. Rev. B* **87**, 024419 (2013).

⁶ W. Schiessl, W. Potzel, H. Karzel, M. Steiner, G. M. Kalvius, A. Martin, M. K. Krause, I. Halevy, J. Gal, W. Schäfer, G. Will, M. Hillberg, and R. Wäppling, *Phys. Rev. B* **53**, 9143 (1996).

⁷ K. M. Rabe, *Annu. Rev. Condens. Matter Phys.* **1**, 211 (2010).

⁸ J. M. Hastings and L. M. Corliss, *Phys. Rev.* **102**, 1460 (1956).

⁹ M. K. Fayek, J. Leciejewicz, A. Murasik, and I. I. Yamzin, *physica status solidi* **37**, 843 (1970).

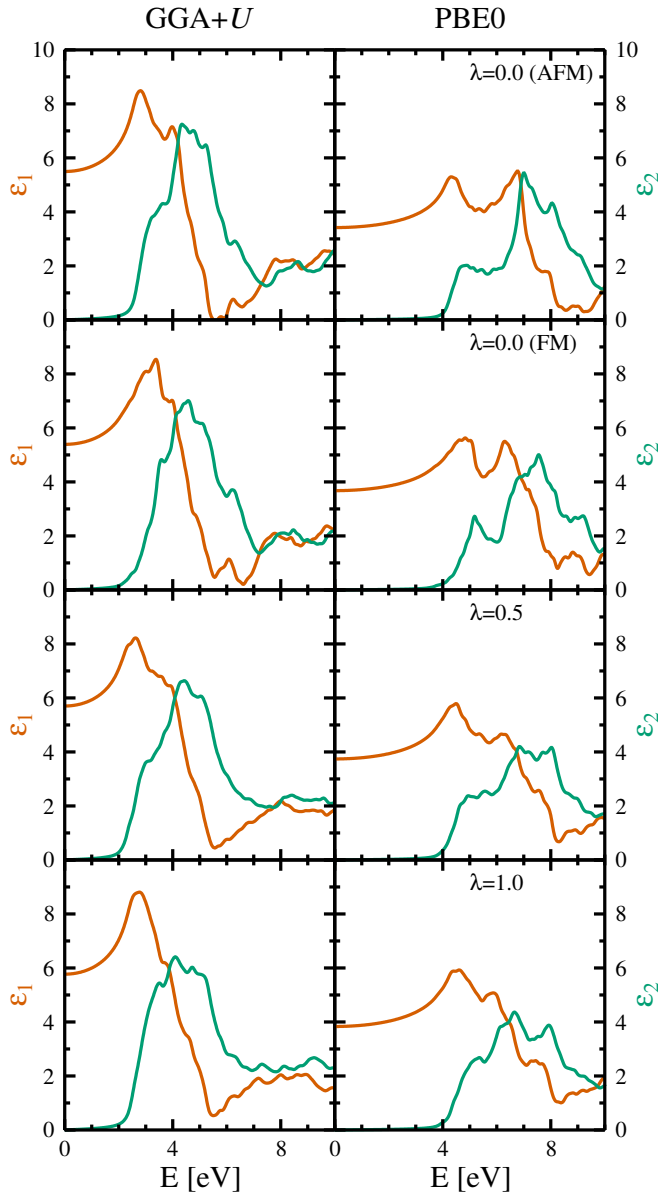


FIG. 3. (Color online) Real (red) and imaginary (green) part of the dielectric functions for ZFO calculated with the GGA+ U (left panels) and PBE0 (right panels) exchange-correlation functionals for different inversion degrees λ and arrangements of the magnetic moments among the B-site sublattice, respectively.

¹⁰ B. Boucher, R. Buhl, and M. Perrin, *physica status solidi* **40**, 171 (1970).
¹¹ U. König, E. F. Bertaut, Y. Gros, M. Mitrikov, and G. Chól, *Solid State Communications* **8**, 759 (1970).
¹² K. Kamazawa, Y. Tsunoda, H. Kadowaki, and K. Kohn, *Phys. Rev. B* **68**, 024412 (2003).
¹³ L. Néel, *Ann. Phys. (Paris)* **3**, 137 (1948).
¹⁴ M. Bohra, S. Prasada, N. Kumar, D. S. Misra, and S. C. Sahoo, *Appl. Phys. Lett.* **88**, 262506 (2006).
¹⁵ T. Böntgen, K. Brachwitz, R. Schmidt-Grund, M. Lorenz, and M. Grundmann, *J. Appl. Phys.* **113**, 073503 (2013).

¹⁶ C. Jin, P. Li, W. Mi, and H. Bai, *J. Appl. Phys.* **115**, 213908 (2014).
¹⁷ E. Lišková-Jakubisová, Š. Višňovský, P. Široký, D. Hrabovský, J. Pištorá, S. C. Sahoo, S. Prasad, N. Venkataramani, M. Bohra, and R. Krishnan, *J. Appl. Phys.* **117**, 17B726 (2015).
¹⁸ S. Ayyappan, S. P. Raja, C. Venkateswaran, J. Philip, and B. Raj, *Appl. Phys. Lett.* **96**, 143106 (2010).
¹⁹ J. Wu, N. Li, J. Xu, Y. Jiang, Z.-G. Ye, Z. Xie, and L. Zheng, *Appl. Phys. Lett.* **99**, 202505 (2011).
²⁰ V. Zviagin, Y. Kumar, I. Lorite, P. Esquinazi, M. Grundmann, and R. Schmidt-Grund, *Appl. Phys. Lett.* **108**, 131901 (2016).
²¹ V. Ziaei and T. Bredow, *Eur. Phys. J. B* **90**, 29 (2017).
²² C. Cheng, *Phys. Rev. B* **78**, 132403 (2008).
²³ S. Soliman, A. Elfalaky, G. H. Fecher, and C. Felser, *Phys. Rev. B* **83**, 083205 (2011).
²⁴ C. E. R. Torres, G. A. Pasquevich, P. M. Zélis, F. Golmar, S. P. Heluani, S. K. Nayak, W. A. Adeagbo, W. Hergert, M. Hoffmann, A. Ernst, P. Esquinazi, and S. J. Stewart, *Phys. Rev. B* **89**, 104414 (2014).
²⁵ C. J. O'Brien, Z. Rák, and D. W. Brenner, *J. Phys.: Condens. Matter* **25**, 445008 (2013).
²⁶ A. D. Rowan, C. H. Patterson, and L. V. Gasparov, *Phys. Rev. B* **79**, 205103 (2009).
²⁷ G. Kresse and J. Hafner, *Phys. Rev. B* **47**, 558 (1993).
²⁸ G. Kresse and J. Hafner, *Phys. Rev. B* **49**, 14251 (1994).
²⁹ G. Kresse and J. Furthmüller, *Comp. Mat. Sci.* **6**, 15 (1996).
³⁰ P. E. Blöchl, *Phys. Rev. B* **50**, 17953 (1994).
³¹ V. I. Anisimov, J. Zaanen, and O. K. Andersen, *Phys. Rev. B* **44**, 943 (1991).
³² J. P. Perdew, K. Burke, and M. Ernzerhof, *Phys. Rev. Lett.* **77**, 3865 (1996).
³³ C. Adamo and V. Barone, *J. Chem. Phys.* **110**, 6158 (1999).
³⁴ S. L. Dudarev, G. A. Botton, S. Y. Savrasov, C. J. Humphreys, and A. P. Sutton, *Phys. Rev. B* **57**, 1505 (1998).
³⁵ A. Manikandan, L. J. Kennedy, M. Bououdina, and J. J. Vijaya, *J. Magn. Magn. Mat.* **349**, 249 (2014).
³⁶ D. Peeters, D. H. Taffa, M. M. Kerrigan, A. Ney, N. Jöns, D. Rogalla, S. Cwik, H.-W. Becker, M. Grafen, A. Ostendorf, C. H. Winter, S. Chakraborty, M. Wark, and A. Devi, *ACS Sustainable Chem. Eng.* **5**, 2917 (2017).
³⁷ D. Gutiérrez, M. Foerster, I. Fina, J. Fontcuberta, D. Fritsch, and C. Ederer, *Phys. Rev. B* **86**, 125309 (2012).
³⁸ D. Fritsch and C. Ederer, *Appl. Phys. Lett.* **99**, 081916 (2011).
³⁹ D. Fritsch and C. Ederer, *Phys. Rev. B* **86**, 014406 (2012).
⁴⁰ J. C. Waerenborgh, M. O. Figueiredo, J. M. P. Cabral, and L. C. J. Pereira, *J. Solid State Chem.* **111**, 300 (1994).
⁴¹ J. M. Hastings and L. M. Corliss, *Rev. Mod. Phys.* **25**, 114 (1953).
⁴² H. J. Reichmann, S. D. Jacobsen, and T. B. Ballaran, *Am. Mineral.* **98**, 601 (2013).
⁴³ D. Fritsch, B. J. Morgan, and A. Walsh, *Nanoscale Research Letters* **12**, 19 (2017).
⁴⁴ D. Fritsch and C. Ederer, *J. Phys.: Conf. Ser.* **292**, 012014 (2011).